


Magnetic dipole effects on non-Newtonian ferrofluid over a stretching sheet

Hussan Zeb¹  | Hafiz A. Wahab¹ | Umar Khan¹ |
Ali J. Chamkha²

¹Department of Mathematics, Hazara University, Mansehra, Pakistan

²Faculty of Engineering, Kuwait College of Science and Technology, Doha District, Kuwait

Correspondence

Hafiz A. Wahab, Department of Mathematics, Hazara University, Mansehra, Pakistan.
Email: wahab@hu.edu.pk

Abstract

In this study, we analyzed the characteristics of heat transfer in non-Newtonian ferrofluids produced by stretchable sheet. Further, we investigated in this study the effects of Arrhenius activation energy and magnetic dipole. We use in this study, a similarity ansatz to simplify the governing system into a nonlinear coupled ordinary differential equations system. We determined the computational solution of the resulting ordinary differential system by applying method with Runge–Kutta method. The influence of beneficial physical parameters on momentum, energy, and concentration profile are shown through graphs. The major finding of this study, the variation of velocity field is reduces for the higher values of M , β , and H . The temperature field increases for higher values of R , and reduce for Pr . Further, we conclude in this study the arising or reducing in the concentration, temperature, and velocity field for various physical parameters. The impacts of physical quantities namely skin fraction, Nusselt, and Sherwood numbers are examined through numerically via tables.

KEYWORDS

activation energy, Eyring–Powell ferrofluid, heat and mass transfer, magnetic dipole

Abbreviations: ABC, a black cat; DEF, does not ever fret; GHI, goes home immediately.

Hafiz A. Wahab contributed equally.

1 | INTRODUCTION

The boundary layer fluids are characterized into Newtonian and non-Newtonian fluids. The Newtonian fluids in which the stress is linearly proportional to the strain. Such examples of Newtonian fluids are mineral oil, water, gasoline, organic matter, kerosene, solvents, glycerin, alcohol, and so on. The boundary layer flow of non-Newtonian fluids is becoming famous due to the enormous range of uses in industries, manufacturing processes and geothermal engineering. These applications including in nuclear reactors, metallurgical processes, spinning of fibers, casting, liquid metals space technology, and crystal growth, and so on. Such examples of non-Newtonian fluids models are plastics polymer, optical fibers, hot rolling, drilling mud, cooling of metallic plates, paper production, and metal spinning. It is a fact that in contrast to Newtonian fluids, Newtonian (Navier–Stokes equation) fluid flow cannot be expressed by a single reference equation. This is due to the properties of Newtonian fluid physics. It is due to the fact of rheological feature of the non-Newtonian fluids. The non-Newtonian fluid materials due to a stretching/shrinking/movable surface/sheet/plates got a huge achievement due to its large number of applications. The properties of non-Newtonian can be examined due to its elasticity, but sometimes rheological properties of fluid are identified by their constitutive equations. Generally, non-Newtonian fluids are categorized in three classes such as (i) rate type, (ii) differential type, and (ii) integral type. Carreau fluid, Maxwell fluid, Oldroyd-B, and Burger fluids and Eyring–Powell fluids are the non-Newtonian fluids. Many authors investigated the non-Newtonian fluid different models can be seen in Hamid and colleagues.^{1–4} Here the focus of this study is to examine the Eyring–Powell fluid.

The Powell–Eyring fluid materials have many benefits in using at low and high shear rates and they formed a Newtonian fluid via the formulation of kinetic theory. It is an interesting topic due to the application of non-Newtonian model in chemical engineering processes. Further, it suitably covers Newtonian performance at high and low shear rates. Human blood, ketchup, toothpaste, and so on are examples of Powell–Eyring fluid. Ghaffar et al.⁵ reported the computational approaches for the effects of heat convection on Eyring–Powell fluid over a vertical surface. Powell–Eyring fluid model^{6–9} is consequent from the kinetic theory of gases instead of realistic relation as in the case of generalized fluids materials. Eyring–Powell fluid past a three-dimensional (3D) stretching surface was presented by Hayat et al.¹⁰ Also Hayat et al.¹¹ presented the impacts of convective boundary conditions and thermal radiation on Powell–Eyring fluid over a moving surface. Najeeb et al.¹² expressed the homotopy solution for Eyring–Powell fluid flow with nanoparticles over a vertical channel. Hina et al.¹³ analyzed the effects of viscose dissipation and thermophysical on Powell–Eyring fluid along the curved channels with nanoparticles. Taseer et al.¹⁴ reported the significance of Arrhenius activation energy on 3D flow of Eyring–Powell fluid with nonlinear thermal radiation. Nisar et al.¹⁵ illustrated the activation energy in heat and mass transfer of Eyring–Powell fluid along the non-linear stretching sheet. The non-linear thermoradiation heat flux in time-dependent flow of an Eyring–Powell fluid with variable thermophysical effects were reported by khatshwa et al.¹⁶ The numerical approximation for stratified magnetic field flow of a non-Newtonian fluid over the included stretching surface was computed by Bilal et al.¹⁷

Heat and mass transfer got attention due to a wide range of applications in chemical industries and many manufacturing processes. For example, space heating, air conditioning, control generation, and refrigeration are well-known applications in engineering. Moreover, this type also includes the transport of certain drugs spread in food processing, distillation, oil distribution, and transport phenomena in the blood (drug delivery) found in many processes.

These applications motivate engineers and scientists to examine heat and mass transfer phenomena theoretically and experimentally. Numerous investigations on mass transfer also establish in living matter phenomena, like sweating, respiration, and nutrition, and so on. There have been studied in the past highlighting role of chemical reaction in mass transfer phenomena see in Bilal et al. and colleagues.^{18–21} and has a variety of uses in nuclear reactor cooling, thermal oil recovery, geothermal reservoirs, and chemical manufacturing industries. Chin et al.²² analyzed 3D Fourier heat flux in rotating magnetic field flow of a Maxwell fluid under the impacts of the binary chemical reaction and activation energy. The numerical approaches for the heat transfer phenomenon of $\text{Al}_2\text{O}_3\text{-H}_2\text{O}$ nanofluid was investigated by Sheikholeslami et al. and colleagues.^{23–25} By applying the Galerkin finite element analysis of the effects of change in temperature and diffusion on steady flow of Casson fluid was calculated by Qureshi et al.²⁶ Sheikholeslami et al.^{27–29} utilized the application of heat transfer behavior of nanoparticle and PCM solidification through an enclosure with thermal energy storage. The heat and mass transfer phenomena on the magnetohydrodynamic (MHD) flow of viscoelastic fluid, over a stretching surface along with Soret and Dufour were studied by Rashidi et al.³⁰

The investigation of chemically reacting processes includes the species of chemical reactants with activation energy, for example invoking in oil reservoir engineering, geothermal, and oil in water emulsions. The relations between chemical reactions and mass transport are commonly very complex and can be observed in the manufacture and consumption of reactant species at different rates in the fluid mass transfer. The initial study of binary chemical reaction and the activation energy was analyzed by Bestman³¹ he also presents the perturbation approaches for the effects natural convection in a porous medium. The activation energy effects on time heat transfer in the rotating flow were presented by Shafique et al.³² The characteristics of activation energy on the rotating mass transfer in time-dependent flow was reported by Awad et al.³³ The activation energy in Newtonian and non-Newtonian see in Kishan et al. and colleagues.^{34–36}

Ferrofluids are colloid materials which are prepared by the suspension of ferromagnetic particles in a nonconducting carrier fluids with low viscosity. Initially ferromagnetic fluids are invented by Stephen³⁷ in 1965. Without the magnetic force these fluids have properties like usual liquids. Ferromagnetic fluids have a remarkable application in chemical industries and modern technology. Some application of these fluids which is in electromechanical devices as commercially, for example, for instance, electric engines, transformers, generates rotating X-ray tubes, hard disks, electromagnets, generators, cure arthritis, spondylitis, gout, headaches and hoarding (recording procedures and hard plates), which is used in biological sciences. The combined impact magnetic field and thermal radiation on the viscose flow of ferrofluid were reported by Neuringer et al.³⁸ The approximate solution for the effect of the magnetic dipole on ferrofluid over a stretching surface are analyzed by Sharma et al.³⁹ heat transfer phenomena and magnetic dipole in a ferrofluid flow over a stretching surface was identified by Majeed et al.⁴⁰ The combined effects of magnetic dipole and stratification on ferrofluid with stagnation point over a stretching sheet were reported by Noor et al.⁴¹ Nonlinear thermal radiating flow of ferrofluids over a moving plat with magnetic dipole effects was identified by Ali et al.⁴² Sajjad⁴³ reported the effect of the magnetic dipole on a non-Newtonian fluid and heat transfer over a stretching surface with Ohmic Dissipation effects. Shehzad et al.⁴⁴ identified the analysis of Cattaneo and Christov heat flux in ferromagnetic fluid with titanium nanoparticles effects. The related work of ferrofluid can be seen in Nadeem and colleagues.^{45–51}

The above literature review is to insure, the aims of current works to present the influence of the magnetic dipole and variable thermal conductivity on the non-Newtonian ferrofluids by considering permeable stretching sheets. As we know that the analytic solution to these kinds of fluid flow problems is not possible, we approximate this numerically. There are various transformations used for fluid flow problems such as scaling group transformations, similarity transformations, and Lie's group transformation. Here in this study we used the similarity transformation to transform the governing model to a coupled nonlinear ordinary differential equations (ODEs) system. We solve the resulting nonlinear ODEs solved by shooting method with RK-method.

2 | MATHEMATICAL MODEL

Considering two-dimensional (2D) flow Eyring-Powell ferrofluids with heat and mass transfer over a stretching surface under the effects activation energy. Further, we take the effects of magnetic dipole and variable thermal conductivity. The sheet is to be considered along with (x, y) with the velocity component (u, v) respectively, it is taken into account normal to the surface seen in Figure 1. Here place a magnetic dipole with the center y -axis by the displacement γ_1 from the sheet. The magnetic dipole is assumed along the positive x -axis. The magnetic field strength is arising because of leading the magnetic dipole is situated to ferrofluids. Here consider the nonuniform temperature at the surface represent by T_w and T_c represent the Curie temperature, whereas the fluid element are considered to be the ambient temperature $T_c = T_\infty$. So it is unable to magnetize until they start to cool upon entering the surface of the boundary layer region.

The consideration of the rate process is to determine the non-Newtonian flow of an Eyring Powell model (1994) is to investigate. Hayat et al.^{10,11} also considered the shear stress of an Eyring Powell fluid model as follows

$$\tau_{i,j} = \mu \frac{\partial u_i}{\partial u_j} + \frac{1}{\Gamma} \sinh^{-1} \left(\frac{1 \partial u_i}{b \partial u_j} \right), \quad (1)$$

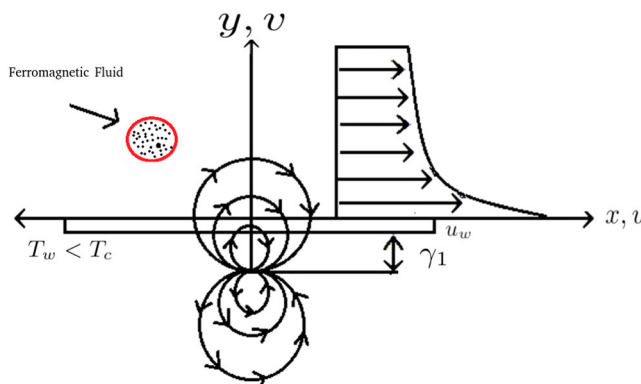


FIGURE 1 Geometrical configuration, the circles configure the magnetic dipole

where μ is taken for viscosity, Γ and b are the fluid materials parameters. We use the second order approximation as follows

$$\sinh^{-1}\left(\frac{1\partial u_i}{b\partial u_j}\right) \cong \frac{1}{b}\left(\frac{\partial u_i}{\partial u_j}\right) - \frac{1}{6b^3}\left(\frac{\partial u_i}{\partial u_j}\right)^3 \quad (2)$$

by implementing the above assumption and the boundary layer approximation to the governing fluid model^{35,52,53} (Eyring–Powell fluid ferrofluid with heat and mass transfer under the effects magnetic dipole) are stated from Equations (3) to (6) as follows:

$$\frac{\partial v}{\partial y} + \frac{\partial u}{\partial x} = 0, \quad (3)$$

$$\frac{\partial u}{\partial y}v + \frac{\partial u}{\partial x}u = -\frac{1}{\rho}\frac{\partial P}{\partial x} + \frac{\mathcal{M}\mu_o}{\rho}\frac{\partial \mathcal{H}}{\partial x} + \left(\nu + \frac{1}{\rho\Gamma b}\right)\frac{\partial^2 u}{\partial y^2} - \frac{1}{2\rho\Gamma b^3}\left(\frac{\partial u}{\partial y}\right)^2\left(\frac{\partial^2 u}{\partial y^2}\right), \quad (4)$$

$$\frac{\partial T}{\partial y}v + \frac{\partial T}{\partial x}u + T\frac{\mu_o}{\rho C_p}\frac{\partial \mathcal{M}}{\partial T}\left(\frac{\partial \mathcal{H}}{\partial x}u + \frac{\partial \mathcal{H}}{\partial y}v\right) = \frac{\kappa}{\rho C_p}\frac{\partial^2 T}{\partial y^2} - \frac{1}{\rho c_p}\frac{\partial q_r}{\partial y}, \quad (5)$$

$$v\frac{\partial C}{\partial y} + u\frac{\partial C}{\partial x} = D\frac{\partial^2 C}{\partial y^2} - \Gamma_2. \quad (6)$$

here in an above calculation (u, v) are represent the velocity components along the (x, y) axis respectively, while C, T, ρ , are taken for the concentration, temperature, density of the base fluid. Further μ, μ_o, k , and k_r are taking for dynamic viscosity, magnetic permeability, thermal conductivity and chemical reaction parameter respectively, subjected to the boundary conditions

$$u(x, y) = u_w(x) = bx, v(x, y) = 0 \quad - T = T_w = T_c - \mathcal{A}\left(\frac{x}{\beta_1}\right)^2, -D\frac{\partial C}{\partial y} = h(C_w - C),$$

$$\text{at } y = 0,$$

$$u(x, y) \rightarrow 0, \frac{\partial u}{\partial y} \rightarrow 0, T \rightarrow T_\infty \quad C \rightarrow C_\infty \quad \text{as } y \rightarrow \infty. \quad (7)$$

The thermal radiation term in Equation (5) is obtained in Rosseland⁵⁴ as

$$\tilde{q}_r = -\frac{4\zeta}{3d^*}\frac{\partial T^4}{\partial y}. \quad (8)$$

Here d^* denotes mean absorption coefficient and ζ specifies the Stefan Boltzman constant. Assume that the relation between of the fluid temperature and the fluid temperature far away from the surface is considered to be a linear function. By using Taylor expansion of T^4 about T_∞ we obtained

$$T^4 \approx 4T_\infty^3 T - 3T_\infty, \quad (9)$$

substituting Equation (9) in (8) we get,

$$\tilde{q}_r = \frac{4\zeta}{3d^*} T_\infty^3 \frac{\partial T}{\partial y}. \quad (10)$$

The Arrhenius term in Equation (6) was analysed by Arrhenius^{35,55}

$$\Gamma_2 = Kr(C - C_\infty) \left(\frac{T}{T_\infty} \right)^n \exp\left(\frac{-E}{\zeta T} \right),$$

where $\zeta = 8.61 \times 10^{-5} \text{eV}$ is assigned for Boltzmann constant, while n stands for unit less exponent fitted rate parameter which generally lies in the range $(-1 < n < 1)$ and E is assigned for activation energy.

3 | MAGNETIC DIPOLE

The influence of magnetic dipole by the effects of magnetic field. Some variation can be prescribed by the well-known function so-called a magnetic scalar potential can be seen Neuringer and colleagues,^{38,40,56} it can be formulated as

$$\Phi = \frac{\gamma_2}{2\pi} \frac{x}{x^2 + (y + \gamma_1)^2} \quad (11)$$

here γ_2 represents the strength of the magnetic field, \mathcal{H}_x and \mathcal{H} are assigned for the magnetic field intensity along the (x, y) axis, it can be written as

$$\mathcal{H}_x = -\frac{\partial \Phi}{\partial x} = \frac{\gamma_2}{2\pi} \frac{-(\gamma_1 + y)^2 + x^2}{((\gamma_1 + y)^2 + x^2)^2}, \quad (12)$$

$$\mathcal{H}_y = \frac{\partial \Phi}{\partial y} = \frac{\gamma_2}{2\pi} \frac{2x(\gamma_1 + y)}{((\gamma_1 + y)^2 + x^2)^2}. \quad (13)$$

Generally is known as the magnetic body force which is gradient of magnetic field \mathcal{M} , it can be formulated as

$$\mathcal{H} = \sqrt{\left(\frac{\partial \Phi}{\partial x} \right)^2 + \left(\frac{\partial \Phi}{\partial y} \right)^2}, \quad (14)$$

invoking Equation (11) and (13) in (14), it gives as follows

$$\frac{\partial \mathcal{H}}{\partial x} = -\frac{\gamma_2}{\pi} \frac{x}{(y + \gamma_1)^4}, \quad (15)$$

$$\frac{\partial \mathcal{H}}{\partial y} = \frac{\gamma_2}{\pi} \left(\frac{2x}{(y + \gamma_1)^5} - \frac{1}{(y + \gamma_1)^3} \right), \quad (16)$$

Consider the magnetization \mathcal{M} as a linear relation the temperature it is given by

$$\mathcal{M} = K_p(T_c - T). \quad (17)$$

The physical and geometrical representation of the ferrofluids is shown in Figure 1.

4 | SIMPLIFICATION OF THE PROBLEMS

By introducing the dimensionless variables as follows:

$$\begin{aligned} \varphi(\eta, \zeta) &= \eta \frac{\mu}{\rho} f(\zeta), \quad \vartheta(\eta, \zeta) = \frac{T_c - T}{T_\infty - T_0} = \vartheta_1(\eta) + \zeta^2 \vartheta_2(\eta) \quad P(\eta, \zeta) = \frac{P}{\mu b} \\ &= P_1(\eta) + \zeta^2 P_2(\eta) \end{aligned} \quad (18)$$

here the dimensional coordinates are defined as

$$\zeta = x \sqrt{x \frac{\rho N}{\mu}}, \quad \eta = y \sqrt{\frac{\rho N}{\mu}}, \quad (19)$$

where $\varphi(\eta, \zeta)$, $\vartheta(\eta, \zeta)$, and $\mathcal{P}(\eta, \zeta)$ the dimensionless stream function, pressure, and temperature, respectively. The velocity is expressed as

$$u = \frac{\partial \varphi^*}{\partial y} = N f'(\eta), \quad v = -\frac{\partial \varphi^*}{\partial x} - \sqrt{\frac{\mu N}{\rho}} f(\eta), \quad (20)$$

by using the similarity transformation (18)–(20) and (11)–(17) in (3)–(6) it reduced to highly nonlinear ODEs which is defined as

$$\begin{aligned} ff''' - f'^2 + 2\mathcal{P}_2 + (H + 1)f''' - \frac{2\beta\vartheta_1}{(\alpha + \eta)^2} - H \Re f''^2 f''' &= 0, \\ \mathcal{P}'_1 - f'' - ff' - \frac{2\beta\vartheta_1}{(\alpha + \eta)^3} &= 0, \\ \mathcal{P}'_2 - \frac{2\beta\vartheta_1}{(\alpha + \eta)^3} + \frac{4\beta\vartheta_1}{(\alpha + \eta)^5} &= 0, \\ (1 + R)\vartheta'_1 + Pr(f\vartheta'_1 - 2f'\vartheta'_1) + 2f\frac{\beta\lambda_1(\vartheta_1 - \epsilon)}{(\alpha + \eta)^3} &= 0, \\ (1 + R)\vartheta'_2 - Pr(f\vartheta'_2 + 4f'\vartheta'_2) + 2f\frac{\beta\lambda_1(\vartheta_2 - \epsilon)}{(\alpha_2 + \eta)^3} + -\lambda_1\beta(\vartheta_1 - \epsilon) \\ \left[\frac{2f'}{(\alpha + \eta)^3} - \frac{4f}{(\alpha + \eta)^5} \right] \\ \varphi'' + Scf\varphi' - ScKr((1 + \delta(\vartheta_1 + \lambda_1\vartheta_2))^n \exp\left(\frac{-E}{(1 + \delta(\vartheta_1 + \lambda_1\vartheta_2))}\right))\varphi &= 0, \end{aligned} \quad (21)$$

the boundary and initial condition become

$$\begin{aligned} f'(\eta) = 1, f(\eta) = 0, \vartheta_1(\eta) = 1, \quad \vartheta_2(\eta) = 0, \phi \rightarrow 0 \text{ at } y = 0. \\ f' \rightarrow 0, \vartheta_1 \rightarrow 0, \vartheta_2 \rightarrow \mathcal{P}_\infty, \quad \mathcal{P}_1 \rightarrow 0, \phi \rightarrow 0, \text{ at } y \rightarrow \infty. \end{aligned} \quad (22)$$

in the above calculation f', ϑ_1, ϕ are represent the dimensionless form of the velocity, temperature, and concentration, respectively. Further β, ϵ , and λ_1 are represent magnetic dipole parameter, is the Curie temperature parameter and viscous dissipation parameter, respectively. $K_r = \frac{k_0}{a}$ is parameter of reaction rate and $Sc = \frac{\nu}{D_B}$ is the Schmith number, $H = \frac{1}{\mu\Gamma b}$ and $\beta = \frac{\rho u_w}{2xb^2\mu}$ are fluid parameters and $Pr = \frac{\mu C_p}{k_\infty}$ is Prandtl number. $K_a = \frac{\gamma_1 a_0^2}{d}$ is denotes the strength of homogeneous (surface) reaction, $\delta_1 = \frac{D_B}{D_A}$ ratio of diffusion coefficient and $Sc = \frac{\nu}{D_B}$ is the Schmith number, $H = \frac{1}{\mu\Gamma b}$ and $\beta = \frac{\rho u_w}{2xb^2\mu}$ are fluid parameters and $Pr = \frac{\mu C_p}{k_\infty}$ is Prandtl number. Further, $\lambda_1 = \frac{d\mu^2}{gk(T_w - T_\infty)}$ is the viscous dissipation parameter, $\epsilon = \frac{T_c}{T_c - T_w}$ is the Curie temperature $\beta = \gamma_1 g \mu_0 \frac{k(T_c - T_w)}{2\pi\mu^2}$ is the ferromagnetic parameter and $\alpha = \gamma_1 \sqrt{\frac{gd}{\mu}}$ be the curvature parameter.

The skin fraction coefficient C_f and Nusselt number Nu_x are expressed as following:

$$\left\{ \begin{aligned} C_f &= \frac{\tau_w}{\rho(u_w)^2}, \\ Nu_x &= \frac{x\tilde{q}_w}{\kappa(T_w - T_\infty)}. \end{aligned} \right. \quad (23)$$

Here q_w is the heat flux, τ_w represents the skin friction along the sheet and j_m is the mass flux from the surface and are given as follows. On the MHD and slip flow over a rotating disk with heat transfer

$$\left\{ \begin{aligned} \tau_w &= \mu \left[\left(1 + \frac{1}{\Gamma b} \right) \frac{\partial \hat{u}}{\partial y} + \frac{1}{\Gamma b^6} \left(\frac{\partial \hat{u}}{\partial y} \right)^3 \right]_{y=0} \\ \tilde{q}_w &= \left[-\kappa \frac{\partial T}{\partial y} - \frac{\partial \tilde{q}_r}{\partial y} \right]_{y=0} \end{aligned} \right. \quad (24)$$

here \tilde{q}_m and u_w are defined as heat transfer and for wall shear stress, respectively. The quantities defined in Equation (16) are transformed into dimensionless form as follows:

$$\left\{ \begin{aligned} C_f \sqrt{Re_x} &= (1 + H)f''(0) - \frac{H\lambda}{3}(f''(0))^3, \\ \frac{Nu_x}{\sqrt{Re_x}} &= - \left[1 + \frac{4}{3}R \right] (\vartheta_1'(0) + \zeta^2 \vartheta_2'(0)). \end{aligned} \right. \quad (25)$$

5 | SHOOTING METHOD FOR THE PROPOSED SOLUTION

The shooting method is a numerical technique, generally, it is used for the solution of nonlinear boundary value problem. Further detail can be seen in the book Esfandiari.⁵⁷ Equation (21) is the system of nonlinear coupled ODE's of order three in $g(\eta)$, order two in $\vartheta(\eta)$ and order two in $\phi(\eta)$ respectively. The rearranging of the Equations (21) with boundary condition in Equation (22) will take the following form:

$$\begin{aligned}
 f''' &= \frac{ff'' - f'^2 + 2P_2 - \frac{2\beta\vartheta_1}{(\alpha + \eta)^2}}{(H + 1) - \beta H f'^2}, \\
 P_1' &= f'' + ff' + \frac{2\beta\vartheta_1}{(\alpha + \eta)^3}, \\
 P_2' &= \frac{2\beta\vartheta_1}{(\alpha + \eta)^3} - \frac{4\beta\vartheta_1}{(\alpha + \eta)^5}, \\
 \vartheta_1'' &= -\frac{Pr(f\vartheta_1' - 2f'\vartheta_1) + 2f\frac{\beta\lambda_1(\vartheta_1 - \epsilon)}{(\alpha + \eta)^3}}{(1 + R)}, \\
 \vartheta_2'' &= -\frac{Pr(f\vartheta_2' - 4f'\vartheta_2) + 2f\frac{\beta\lambda_1(\vartheta_2 - \epsilon)}{(\alpha_2 + \eta)^3} + \lambda_1\beta(\vartheta_1 - \epsilon)\left[\frac{2f'}{(\alpha + \eta)^3} - \frac{4f}{(\alpha + \eta)^5}\right]}{(1 + R)}, \\
 \phi'' &= -(Scf\phi' - ScKr\left((1 + \delta(\vartheta_1 + \lambda_1))^n \exp\left(\frac{-E}{(1 + \delta(\vartheta_1 + \lambda_1\vartheta_2))}\right)\phi\right)),
 \end{aligned} \tag{26}$$

To compute this system we need to transform these coupled ODE's into a system of nonlinear first order ODE's. For this we defined these new variables as follow

$$\begin{aligned}
 f &= u_1, f' = u_2, f'' = u_3, f''' = u_3', \\
 \vartheta_1 &= u_4, \vartheta_1' = u_5, \vartheta_1'' = u_5', \vartheta_2 = u_6, \vartheta_2' = u_7, \vartheta_2'' = u_7', \\
 P_2' &= u(8), P_1' = u(9), \phi = u_{10}, \phi' = u_{11} \text{ and } \phi'' = u_{11}'.
 \end{aligned} \tag{27}$$

By using these we obtained the following nonlinear first-order ODE's system

$$\begin{aligned}
 u_1' &= u_2, \\
 u_2' &= u_3, \\
 u_3' &= -\frac{u_1 u_3 - u_2^2 + 2u_8 - \frac{2\beta u_4}{(\alpha + \eta)^2}}{(H + 1) - \beta H u_3^2}, \\
 u_4' &= u_5, \\
 u_5' &= -\frac{Pr(u_1 u_5 - 2u_2 u_5) + 2u_1 \frac{\beta \lambda_1 (u_4 - \epsilon)}{(\alpha + \eta)^3}}{(1 + R)}, \\
 u_6' &= u_7, \\
 u_7' &= -\frac{Pr(u_1 u_7 - 4u_2 u_7) + 2u_1 \frac{\beta \lambda_1 (u_6 - \epsilon)}{(\alpha_2 + \eta)^3} + \lambda_1 \beta (u_4 - \epsilon) \left[\frac{2u_2}{(\alpha + \eta)^3} - \frac{4u_1}{(\alpha + \eta)^5} \right]}{(1 + R)}, \\
 u_9 &= u_3 + u_1 u_2 + \frac{2\beta u_4}{(\alpha + \eta)^3}, \\
 u_8 &= \frac{2\beta u_4}{(\alpha + \eta)^3} - \frac{4\beta u_4}{(\alpha + \eta)^5}, \\
 u_{10}' &= u_{11}, \\
 u_{11}' &= -(Scu_1 u_{11} - ScKr \left((1 + \delta \delta (u_6 + \lambda_1 u_4))^n \exp \left(\frac{-E}{(1 + \delta (u_6 + \lambda_1 u_4))} \right) u_{10} \right)),
 \end{aligned} \tag{28}$$

In these calculations, the prime indicate the derivative and the transform boundary conditions are given as

$$\begin{aligned}
 u_1 = 0, u_2 = 1, u_3 = S_1, u_4 = 1, \quad u_5 = S_2, \quad u_6 = 0, \\
 u_7 = S_3, u_8 = S_4, \quad u_9 = S_5, \quad u_{10} = 1, \quad u_{11} = S_6 \text{ at } \eta = 0 \\
 u_2 = 0, u_4 = 0, u_6 = 0, u_8 = 0, u_9 = -P_\infty \text{ and } u_{11} = 0 \text{ at } \eta \rightarrow \infty.
 \end{aligned} \tag{29}$$

To evaluate the solution of these seven ODE's system equation (29) with boundary conditions by shooting method, we need 11 initial guesses whereas five of them are given and the other six initial guesses $u_2(\eta)$, $u_4(\eta)$, $u_6(\eta)$, $u_8(\eta)$, $u_9(\eta)$, and $u_{11}(\eta)$ are defined as $\eta \rightarrow \infty$.

TABLE 1 Validation for $\vartheta_1'(0)$ at $H = 0.0$, $R = \beta = \beta = 0$ for Pr with the published work

Pr	Majeed et al. ⁵²	Chen ⁵⁸	Present work
0.72	1.0885	1.08862	1.0886
1.0	1.3333	1.3333	1.3333
3.0	2.5097	2.50972	2.5095
10.0	4.7968	4.79682	4.7943

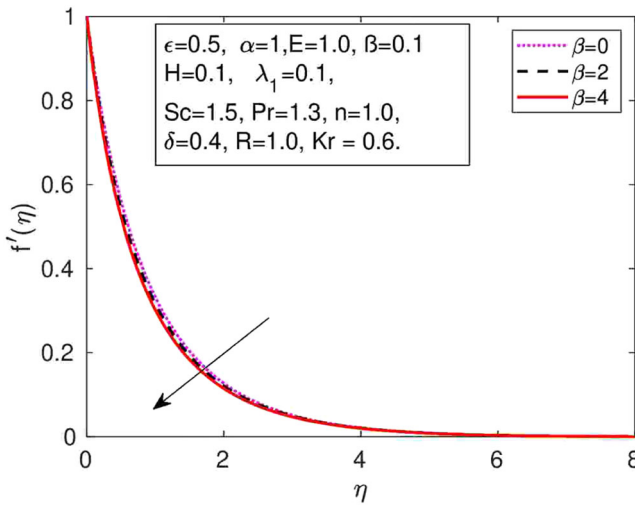


FIGURE 2 Characteristics of β for the velocity distribution f'

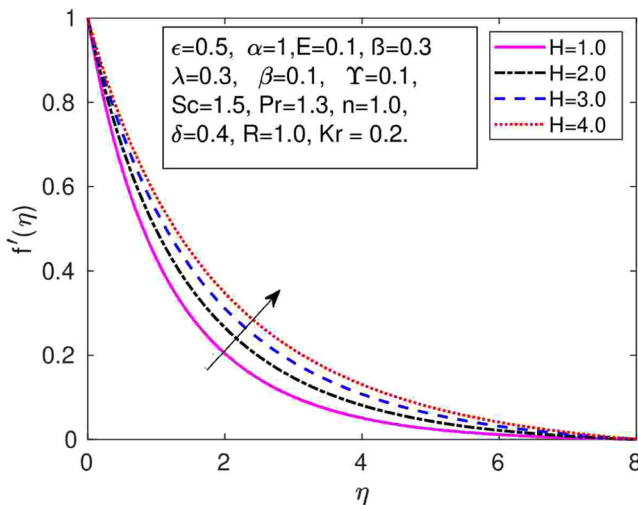


FIGURE 3 The result of H on $f'(\eta)$

Hence it is considered that $(u_3(0), u_5(0), u_7(0), u_8(0), u_9(0), u_{11}(0)) = (q_1, q_2, q_3, q_3, q_5, q_6)$. These unknown six initial guesses $(q_1, q_2, q_3, q_3, q_5, q_6)$ are computed by Newton's iterative scheme through Runge Kutta-method (RK-45). The main step of this numerical solution to select the suitable finite boundary conditions. The step size and convergence criteria are taken $h = 0.02$ and $TOL = 10^{-5}$ respectively, for our numerical solution.

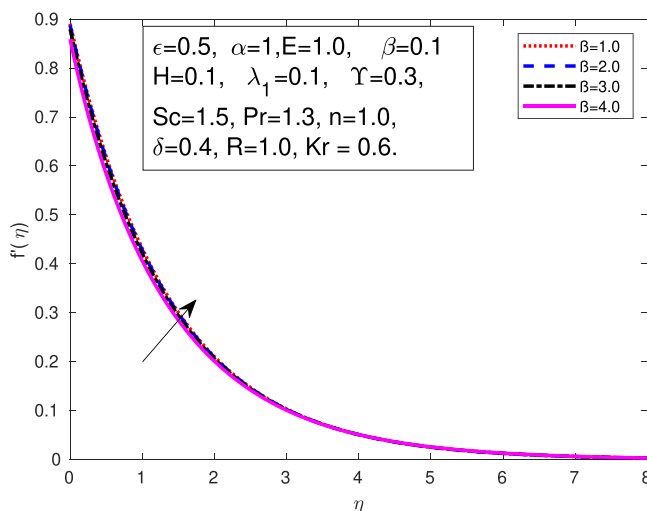


FIGURE 4 The result of β on $f'(\eta)$

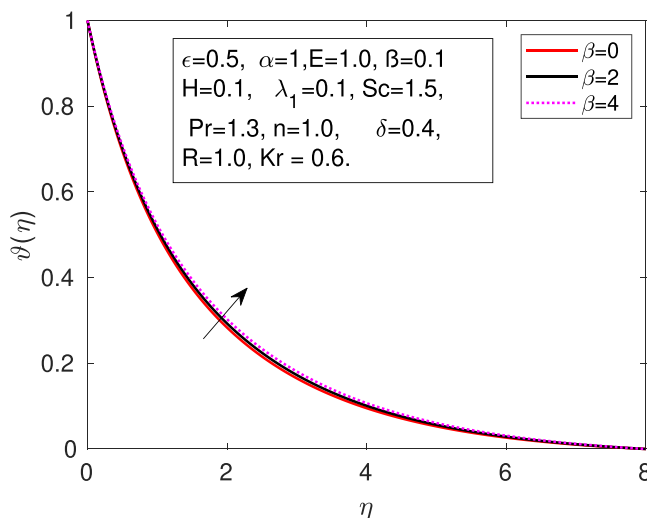


FIGURE 5 The distribution of $\vartheta(\eta)$ for β

6 | VALIDATION OF THE NUMERICAL SOLUTION

In this section, we validate our numerical results with the previously published work. The comparison of $\vartheta_1'(0)$ is shown in Table 1 and we found a good agreement between these two methods. We have to evaluate the accuracy of the current method. For this we computed the different values of Pr . We used a shooting method programming in MATLAB with step size $h = 0.02$ to get the velocity concentration and temperature profiles.

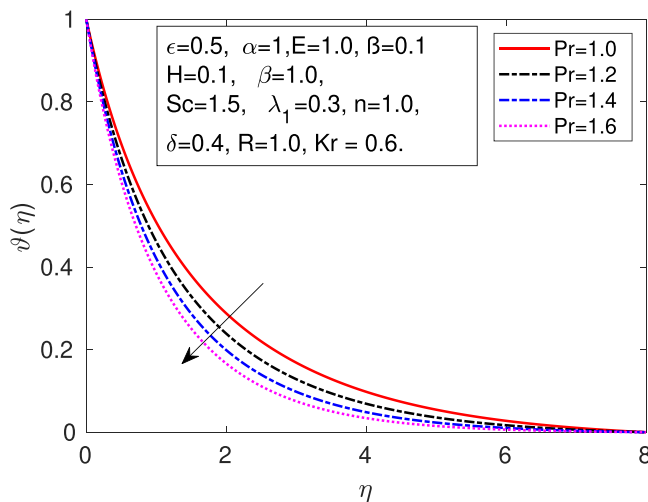


FIGURE 6 The gradient of $\vartheta(\eta)$ for Pr

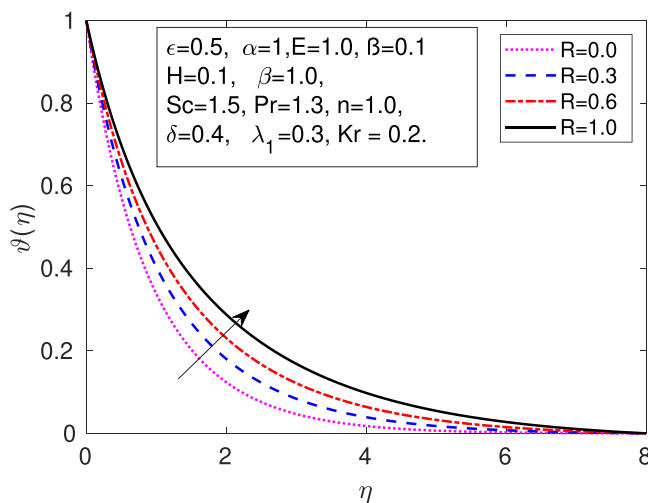


FIGURE 7 The impact of R for $\vartheta(\eta)$

7 | RESULTS AND DISCUSSIONS

In this section, we solved the governing Equations (13)–(15) with shooting method. Here we took $h = 0.002$. The tolerance for the convergence has been taken $TOL = 10^{-5}$. Moreover, we compared the current result with the previously published work see in Table 1. We present the characteristics of parameters involved in Equations (13)–(15). The characteristics of velocity, temperature, and concentration are presents through Figures 2–14. Also the computational result of the skin fraction, heat and mass transfer rate are presented through Table 2.

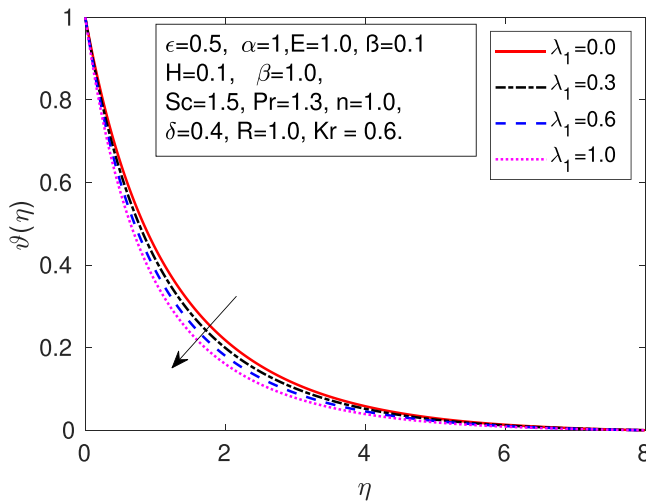


FIGURE 8 The distribution of $\vartheta(\eta)$ for λ_1

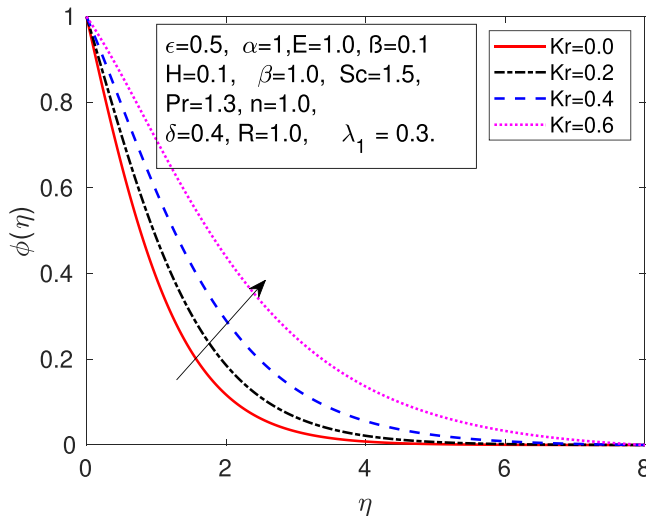


FIGURE 9 Concentration distribution ϕ for Kr . $\phi(\eta)$

The characteristics of ferromagnetic in this model is assumed the dimensionless distance at the center of magnetic dipole and the interaction of ferromagnetic parameter β which is shown in Figure 2. The physical reason behind that it is interaction in the external magnetic dipole and the fluid motion because of the dipole. An arising in the ferromagnetic parameter β have flattening the axial velocity $f'(\eta)$. It is fact that the basically.

Figure 3 represents the velocity field for (material fluid parameter H). It represent increases the variation of velocity profile by enlarge the values of H . Figure 4 demonstrates the velocity profile for β . Clearly it is seen that the impacts for β on the velocity field increases both the film thickness.

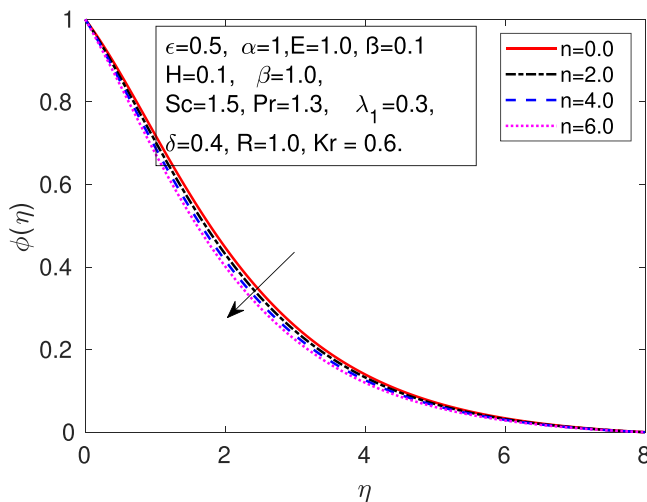


FIGURE 10 The impact of n for ϕ

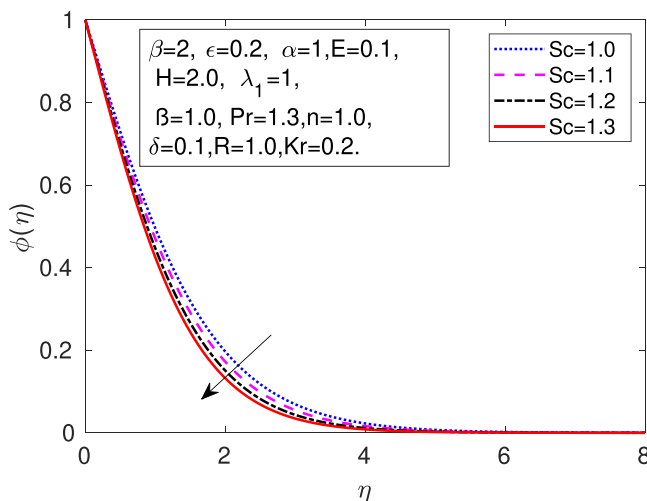


FIGURE 11 The characteristics of Sc for the distribution of $\phi(\eta)$

Figure 5 represents the characteristics of β on the temperature distribution. Here increase occurs in temperature field for higher values of β . This is due to the interaction in the action of ferromagnetic field and the motion of the fluids. Reduces occurs in this interaction for velocity field there by arising the fractional heating in the boundary layers, therefore increases occurs in the thickness of thermal boundary layer.

Figure 6 represents the characteristics of the temperature for the higher values of (Prandtl number Pr). This is due to, the fluid contains a small values of Pr have a high thermal diffusivity. Figure 7 in made for temperature field with the unlike numbers radiation parameter

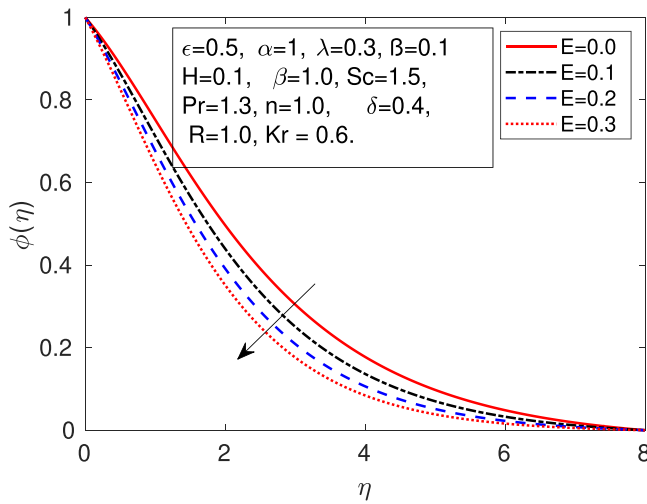


FIGURE 12 The properties of E for the gradient of $\phi(\eta)$

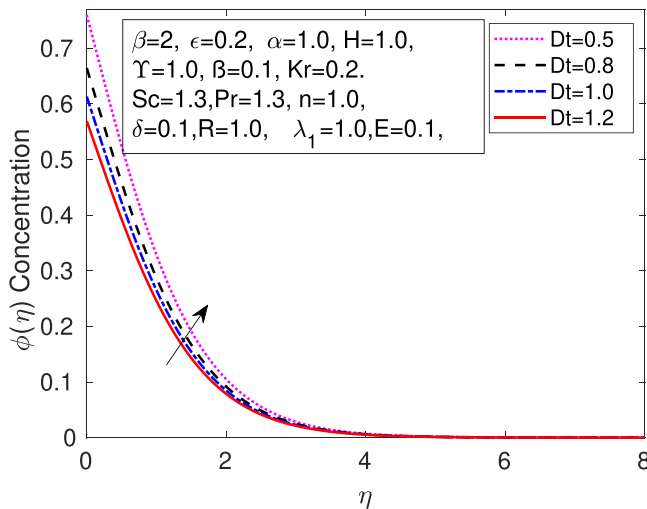


FIGURE 13 The impact of Dt on concentration field $\phi(\eta)$

R . If we increase the values of R then the temperature profile increases. This increase occurs due to the increase in temperature \bar{T}_{∞}^3 in radiation.

Figure 8 demonstrates the characteristics of λ_1 on temperature field. It is seen that from this figure the reduces the temperature by enlarging the values of λ_1 . The physical facts behind the extraordinary characteristics of ferrofluid. However, this is contrary in the case of hydrodynamic ($\beta = 0$) whereas is an arising in the values of λ_1 represents an arises occur in temperature field near to the boundary layer region by enlarging the values of λ_1 .

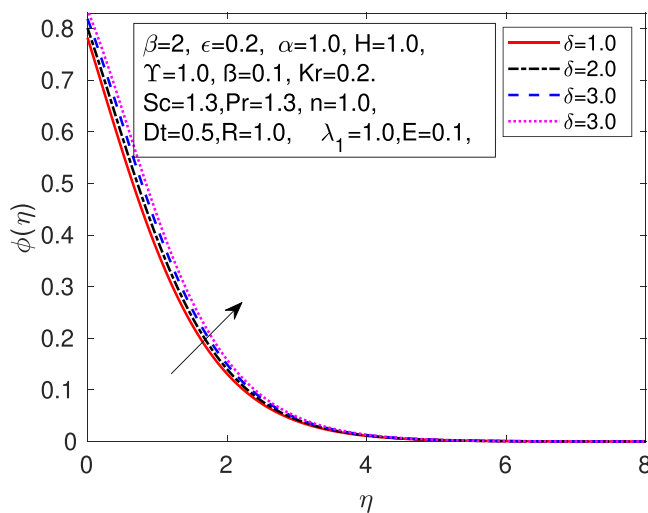


FIGURE 14 The properties of δ for the gradient of $\phi(\eta)$

TABLE 2 The properties of $-f''(0)$, $-\theta'_1(0)$ and $\phi'(0)$ for λ_1 , Pr , β , R , β , E , δ , Kr , H , α , and Dt

Pr	β	λ_1	R	β	E	δ	Kr	H	α	Dt	$-f''(0)$	$-\theta'_1(0)$	$\phi(0)$
1	2	1	1	0.1	0.2	1	0.2	1	1	0.5	1.0441	1.3485	0.43269
											1.0446	1.4716	0.43663
											1.4580	1.5820	0.43962
		1.5									1.0141	1.3629	0.43485
		2.0									1.0441	1.3485	0.43269
		2.5									1.0725	1.3342	0.43059
		1									1.0441	1.3485	0.43269
		1.3									1.0328	1.4632	0.40328
		1.6									1.0218	1.5859	0.04291
		1									1.0441	1.3485	0.43269
		1.3									1.3970	1.2286	0.43041
		1.6									1.0355	1.1310	0.42508
				0.2							1.0141	1.3629	0.43485
				0.3							1.0290	1.3600	0.45234
				0.4							1.0643	1.3538	0.43234
					0.2						1.0441	1.3485	0.43269
					0.4						1.0441	1.3485	0.45099
					0.8						1.0643	1.3538	0.48060

(Continues)

TABLE 2 (Continued)

Pr	β	λ_1	R	β	E	δ	Kr	H	α	Dt	$-f''(0)$	$\vartheta_1(0)$	$\phi(0)$
						1.0					1.0441	1.3485	0.48298
						2.0					1.0441	1.3485	0.43269
						3.0					1.0643	1.3538	0.38492
							0.0				1.0441	1.3485	0.57730
							0.2				1.0441	1.3485	0.48298
							0.4				1.0643	1.3538	0.29763
								1.0			1.0441	1.3485	0.43269
								1.5			0.9204	1.4141	0.44905
								2.0			8.3114	1.4663	0.46071
									1.0		1.0441	1.3485	0.43269
									1.5		0.9624	1.3865	0.43772
									1.8		0.9445	1.3944	0.39010

Figure 9 represents the characteristics of concentration gradient for the (chemical reaction Kr). Here reduces occurs in concentration gradient for the improving numbers of Kr . Here it is observed that decreases the concentration field by the higher number of Kr . Figure 10 reports the distribution of concentration field for fitted rate constant n . The result has shown that, reduces occur in concentration field due to the improving values of fitted rate constant n . Figure 11 designates the concentration gradient for higher values of Sc . The results show that the concentration profile is decreases for by enlarging the values of Sc . Figure 12 demonstrates the influence of (activation energy E) on concentration field ϕ . Here it is seen that the concentration field is improving for higher valves of E . Figure 13 is plotted the characteristics of concentration field for unlike vales of Dt . It is noted that the concentration field arising by higher values of Dt . The properties of (temperature difference parameter δ) on concentration field are shown in Figure 14. Here the result has shows that the reduces occurring in concentration field by larger values of δ .

Table 2 presents the properties of Sherwood numbers, Nusselt numbers, and skin fractions for different physical parameters. Skin friction increases for the higher values of of H and λ_1 . Skin friction is reduced for larger values β and β . Nu_x increases for higher values of H , $R\alpha$, and β . Nu_x Nusselt number is reduced for higher values of R , Pr , and λ_1 . The Sherwood number steps up by higher values of Kr , δ , Dt , and R . Sherwood numbers Sh_x are reduced for the higher values of $\alpha H Pr$, λ_1 , and E .

8 | CONCLUSIONS

In this study we analyzed the effects of activation energy in Eyring–Powell ferrofluid fluid in the existence of magnetic dipole. Further, the impacts of thermal radiation, variables of thermal conductivity, and mass convective boundary conditions are analysed. Here we transformed the governing model into a nonlinear coupled ODEs by using similarity

transformation. We determined the computational solution of the transform ordinary differential system by applying the shooting method with RK-45. The characteristics of (concentration, temperature, and velocity) profiles for various physical parameters are presented through graphs. The behavior of the Sherwood numbers, heat transfer rate, and skin friction coefficients are displayed in tables. In this article, we conclude the following facts.

- The reduction occurs in velocity field $f'(0)$ by enlarging values of β , H and M .
- There is an increase in temperature gradients $\vartheta_1(\eta)$ by the higher values of R and H .
- There are decreases occurring in temperature gradients $\theta(\eta)$ with higher values of Pr .
- There is an increment in concentration field $\phi(\eta)$ for higher values of E .
- There is an increases the concentration field $\phi(\eta)$ for larger values of Sc , Kr , n , and δ .

ORCID

Hussan Zeb  <http://orcid.org/0000-0002-0981-5199>

REFERENCES

1. Hamid M, Usman M, Haq RU, Khan ZH, Wang W. Wavelet analysis of stagnation point flow of non-Newtonian nanofluid. *Appl Math Mech*. 2019;40(8):1211. https://www.amm.shu.edu.cn/EN/abstract/article_16653.shtml
2. Hashim KM, Alshomrani AS, Haq RU. Investigation of dual solutions in flow of a non-Newtonian fluid with homogeneous-heterogeneous reactions: critical points. *Eur J MechaB/Fluids*. 2018;68:30-38. <https://www.sciencedirect.com/science/article/pii/S0997754617301152>
3. Besthapu P, Haq RU, Bandari S, Al-Mdallal QM. Thermal radiation and slip effects on MHD stagnation point flow of non-Newtonian nanofluid over a convective stretching surface. *Neural Comput Appl*. 2019;31(1):207-217.
4. Ibrahim W, Negera M. Viscous dissipation effect on mixed convective heat transfer of MHD flow of Williamson nanofluid over a stretching cylinder in the presence of variable thermal conductivity and chemical reaction. *Heat Transfer*. 2020;50:2427-2453. doi:10.1002/htj.21985
5. Gaffar SA, Prasad VR, Vijaya B. Computational study of non-Newtonian Eyring-Powell fluid from a vertical porous plate with Biot number effects. *J Braz Soc Mech Sci Eng*. 2017;39(7):2747-2765.
6. Powell RE, Eyring H. Mechanism for relaxation theory of viscosity. *Nature*. 1944;154:427-8.
7. Ellahi R, Shivanian E, Abbasbandy S, Hayat T. Numerical study of magnetohydrodynamics generalized Couette flow of Eyring-Powell fluid with heat transfer and slip condition. *Int J Numer Methods Heat Fluid Flow*. 2010;26:1433-1445.
8. EROsca AV, Pop I. Flow and heat transfer of Powell-Eyring fluid over a shrinking surface in a parallel free stream. *Int J Heat Mass Transfer*. 2014;71:231-237.
9. Maleki H, Safaei MR, Togun H, Dahari M. Heat transfer and fluid flow of pseudo-plastic nanofluid over a moving permeable plate with viscous dissipation and heat absorption/generation. *J Thermal Anal Calorimetry*. 2019;135:1643-1654.
10. Hayat T, Awais M, Asghar S. Radiative effects in a three-dimensional flow of MHD Eyring-Powell fluid. *J Egypt Math Society*. 2013;21(3):379-384.
11. Starlin I, Yuen D, Bergeron S. Thermal evolution of sedimentary basin formation with temperature-dependent conductivity. *Geophys Res Lett*. 2000;27(2):265-268.
12. Khan NA, Sultan F, Rubbab Q. Optimal solution of nonlinear heat and mass transfer in a two-layer flow with nano-Eyring-Powell fluid. *Res Phys*. 2015;5:199-205.
13. Hina S, Mustafa M, Hayat T, Alsaedi A. Peristaltic transport of Powell-Eyring fluid in a curved channel with heat/mass transfer and wall properties. *Int J Heat Mass Transfer*. 2016;101:156-165.
14. Muhammad T, Waqas H, Khan SA, Ellahi R, Sait SM. Significance of nonlinear thermal radiation in 3D Eyring-Powell nanofluid flow with Arrhenius activation energy. *J Thermal Anal Calorimetry*. 2020;143:929-944.

15. Nisar Z, Hayat T, Alsaedi A, Ahmad B. Significance of activation energy in radiative peristaltic transport of Eyring-Powell nanofluid. *Int Commun Heat Mass Transfer*. 2020;116:104655.
16. Mkhathshwa MP, Motsa SS, Sibanda P. MHD mixed convective radiative flow of Eyring-Powell fluid over an oscillatory stretching sheet using bivariate spectral method on overlapping grids. *Heat Transfer*. 2021;50(1): 655-687.
17. Bilal M, Nazeer M. Numerical analysis for the non-Newtonian flow over stratified stretching/shrinking inclined sheet with the aligned magnetic field and nonlinear convection. *Archiv Appl Mech*. 2020;91:949-964.
18. Bilal S, Rehman KU, Jamil H, Malik M, Salahuddin T. Dissipative slip flow along heat and mass transfer over a vertically rotating cone by way of chemical reaction with Dufour and Soret effects. *AIP Adv*. 2016;6(12):125125.
19. Mabood F, Shateyi S, Rashidi M, Momoniati E, Freidoonimehr N. MHD stagnation point flow heat and mass transfer of nanofluids in porous medium with radiation, viscous dissipation and chemical reaction. *Adv Powder Technol*. 2016;27(2):742-749.
20. Ahmed S, Zueco J, López-González LM. Effects of chemical reaction, heat and mass transfer and viscous dissipation over a MHD flow in a vertical porous wall using perturbation method. *Int J Heat Mass Transfer*. 2017;104:409-418. <http://www.sciencedirect.com/science/article/pii/S0017931015312242>
21. Kumar RN, Jyothi A, Alhumade H, et al. Impact of magnetic dipole on thermophoretic particle deposition in the flow of Maxwell fluid over a stretching sheet. *J Mol Liquids*. 2021;334:116494.
22. Lu DC, Ramzan M, Bilal M, Chung JD, Farooq U. A numerical investigation of 3D MHD rotating flow with binary chemical reaction, activation energy and non-Fourier heat flux. *Commun Theoretical Phys*. 2018;70(1):89. doi:10.1088/0253-6102/70/1/89
23. Sheikholeslami M. Numerical investigation for CuO-H₂O nanofluid flow in a porous channel with magnetic field using mesoscopic method. *J Mol Liquids*. 2018;249:739-746.
24. Sheikholeslami M, Gerdroodbar MB, Moradi R, Shafee A, Li Z. Application of neural network for estimation of heat transfer treatment of Al₂O₃-H₂O nanofluid through a channel. *Comput Methods Appl Mech Eng*. 2019;344:1-12.
25. Mohsen S. Numerical simulation of magnetic nanofluid natural convection in porous media. *Phys Lett A*. 2017;381(5):494-503.
26. Qureshi IH, Nawaz M, Rana S, Zubair T. Galerkin finite element study on the effects of variable thermal conductivity and variable mass diffusion conductance on heat and mass transfer. *Commun Theor Phys*. 2018;70(1):49.
27. Sheikholeslami M. Finite element method for PCM solidification in existence of CuO nanoparticles. *J Mol Liquids*. 2018;265:347-355.
28. Sheikholeslami M. Numerical modeling of nano enhanced PCM solidification in an enclosure with metallic fin. *J Mol Liquids*. 2018;259:424-438.
29. Wang F, Ali S, Nadeem S, Muhammad N, Nofal TA. Numerical analysis for the effects of heat transfer in modified square duct with heated obstacle inside it. *Int Commun Heat Mass Transfer*. 2021;129:105666.
30. Rashidi MM, Ali M, Rostami B, Rostami P, Xie GN. Heat and mass transfer for MHD viscoelastic fluid flow over a vertical stretching sheet with considering soret and dufour effects. *Math Prob Eng*. 2015;2015:861065.
31. Bestman A. Radiative heat transfer to flow of a combustible mixture in a vertical pipe. *Int J Energy Res*. 1991;15(3):179-184.
32. Shafique Z, Mustafa M, Mushtaq A. Boundary layer flow of Maxwell fluid in rotating frame with binary chemical reaction and activation energy. *Results Phys*. 2016;6:627-633.
33. Awad FG, Motsa S, Khumalo M. Heat and mass transfer in unsteady rotating fluid flow with binary chemical reaction and activation energy. *PloS One*. 2014;9(9).
34. Kishan N, Kalyani C, ChennaKrishnaReddy M. MHD boundary layer flow of a nanofluid over an exponentially permeable stretching sheet with radiation and heat Source/Sink. *Transp Phenom Nano Micro Scales*. 2016;4(1):44-51.
35. Hafiz W, Zeb H, Bhatti S, Gulistan M, Kadry S, Nam Y. Numerical study for the effects of temperature dependent viscosity flow of Non-Newtonian fluid with double stratification. *Appl Sci*. 2020;10(2):708. <https://www.mdpi.com/2076-3417/10/2/708>
36. Mustafa M, Khan JA, Hayat T, Alsaedi A. Buoyancy effects on the MHD nanofluid flow past a vertical surface with chemical reaction and activation energy. *Int J Heat Mass Transfer*. 2017;108:1340-1346.

37. Stephen PS. Low viscosity magnetic fluid obtained by the colloidal suspension of magnetic particles. 1965. US Patent 3,215,572.
38. Neuringer JL. Some viscous flows of a saturated ferro-fluid under the combined influence of thermal and magnetic field gradients. *Int J Non-Linear Mech.* 1966;1(2):123-137.
39. Sharma D, Sharma R, et al. Effect of dust particles on thermal convection in ferromagnetic fluid saturating a porous medium. *J Magnet Magnet Mater.* 2005;288:183-195.
40. Majeed A, Zeeshan A, Ellahi R. Unsteady ferromagnetic liquid flow and heat transfer analysis over a stretching sheet with the effect of dipole and prescribed heat flux. *J Mol Liquids.* 2016;223:528-533.
41. Muhammad N, Nadeem S, Haq RU. Heat transport phenomenon in the ferromagnetic fluid over a stretching sheet with thermal stratification. *Results Phys.* 2017;7:854-861.
42. Ijaz M, Nadeem S, Ayub M, Mansoor S. Simulation of magnetic dipole on gyrotactic ferromagnetic fluid flow with nonlinear thermal radiation. *J Thermal Anal Calorimetry.* 2020;143:2053-2067.
43. Sajjad R, Mushtaq M, Farid S, Jabeen K, Muntazir R. Numerical simulations of magnetic dipole over a nonlinear radiative Eyring-Powell nanofluid considering viscous and ohmic dissipation effects. *Math Prob Eng.* 2021;2021:9776759.
44. Shehzad S, Reddy MG, Vijayakumari P, Tlili I. Behavior of ferromagnetic Fe₂SO₄ and titanium alloy Ti₆Al₄V nanoparticles in micropolar fluid flow. *Int Commun Heat Mass Transfer.* 2020;117:104769.
45. Nadeem S, Raishad I, Muhammad N, Mustafa M. Mathematical analysis of ferromagnetic fluid embedded in a porous medium. *Results Phys.* 2017;7:2361-2368.
46. Ashraf A, Zhang Z, Saeed T, Zeb H, Munir T. Convective heat transfer analysis for aluminum oxide (Al₂O₃)- and ferro (Fe₃O₄)-based nano-fluid over a curved stretching sheet. *Nanomaterials.* 2022;12(7):1152.
47. Abbas N, Malik M, Nadeem S, Alarifi IM. On extended version of Yamada-Ota and Xue models of hybrid nanofluid on moving needle. *Eur Phys J Plus.* 2020;135(2):145.
48. Bailey R. Lesser known applications of ferrofluids. *J Magnet Magnet mater.* 1983;39(1-2):178-182.
49. Andersson H, Valnes O. Flow of a heated ferrofluid over a stretching sheet in the presence of a magnetic dipole. *Acta Mech.* 1998;128(1-2):39-47.
50. Muntazir R, Mushtaq M, Shahzadi S, Jabeen K. Influence of chemically reacting ferromagnetic Carreau nanofluid over a stretched sheet with magnetic dipole and viscous dissipation. *Math Prob Eng.* 2021;2021:1-12.
51. Zeb H, Bhatti S, Khan U, Wahab H, Mohamed A, Khan I. Impact of Homogeneous-Heterogeneous reactions on flow of Non-Newtonian ferrofluid over a stretching sheet. *J Nanomater.* 2022;2022:1-11.
52. Majeed A, Zeeshan A, Ellahi R. Chemical reaction and heat transfer on boundary layer Maxwell ferro-fluid flow under magnetic dipole with sores and suction effects. *Eng Sci Technol Int J.* 2017;20(3):1122-1128.
53. Zeb H, Wahab HA, Khan U, Juhani ASA, Andualet M, Khan I. The velocity slip boundary condition effects on non-Newtonian ferrofluid over a stretching sheet. *Math Prob Eng.* 2022;2022:1-20.
54. Rosseland S. *Astrophysik and atom-theoretische Grundlagen.* Springer; 1993.
55. Reddy S, Reddy PBA, Rashad A. Activation energy impact on chemically reacting Eyring-Powell nanofluid flow over a stretching cylinder. *Arab J Sci Eng.* 2020;45:5227-5242.
56. Zeeshan A, Majeed A, Ellahi R. Effect of magnetic on viscous ferro-fluid past a stretching surface with thermal radiation. *J Mol Liquids.* 2016;215:549-554.
57. Esfandiari SR. *Numerical Methods for Engineers and Scientists Using MATLAB.* CRC Press; 2013.
58. Chen CH. Laminar mixed convection adjacent to vertical, continuously stretching sheets. *Heat Mass Transfer.* 1998; 33(5-6): 471-476.

How to cite this article: Zeb H, Wahab HA, Khan U, Chamkha AJ. Magnetic dipole effects on non-Newtonian ferrofluid over a stretching sheet. *Heat Transfer.* 2023;52:759-779. doi:10.1002/htj.22715